Photoluminescence properties and energy transfer in Y_2O_3:Eu^{3+} nanophosphors*

Cui Hang(崔 航)[a], Zhu Pei-Fen(朱培芬)[b], Zhu Hong-Yang(祝洪洋)[a]†, Li Hong-Dong(李红东)[a], and Cui Qi-Liang(崔啟良)[a]

[a] *State Key Laboratory of Superhard Materials, Jilin University, Changchun* 130012, *China*
[b] *Department of Electrical and Computer Engineering, Lehigh University, Bethlehem, PA* 18015, *USA*

(Received 23 December 2013; revised manuscript received 7 February 2014; published online 1 April 2014)

The photoluminescence (PL) properties of Y_2O_3:Eu^{3+} nanophosphors were systematically investigated with the goal of improving the color quality and quantum efficiency of Y_2O_3:Eu^{3+} nanophosphors for potential applications in nanoscale devices. The emission spectra, excitation spectra and fluorescence decay curves were employed to trace the energy transfer process from Eu^{3+} at C_{3i} site to Eu^{3+} at C_2 site. The experimental results show that the energy transfer process becomes more and more efficient with the increase in the Eu^{3+} concentration. The emission of Eu^{3+} at C_2 site is favorable because it has high radiative efficiency and better color quality. The successful suppress of the emission Eu^{3+} at C_{3i} is especially important for its applications in general illumination or display technology. The quantum efficiency and color quality of Y_2O_3:Eu^{3+} can be improved by controlling the energy transfer between the Eu^{3+} at S_6 site and Eu^{3+} at C_2 site.

Keywords: Y_2O_3:Eu^{3+}, photoluminescence, energy transfer, fluorescence lifetime

PACS: 78.20.–e, 78.60.Lc, 42.70.–a **DOI:** 10.1088/1674-1056/23/5/057801

1. Introduction

Y_2O_3:Eu^{3+} phosphor is a well-known red phosphor, that is widely used in fluorescent lamps, projection televisions, and field emission displays due to its high emission efficiency.[1–7] As we know, the transitions of Eu^{3+} are sensitive to the crystal field environment, which lead to different optical properties of Eu^{3+} at different symmetry sites.[8] Eu^{3+} locate two symmetry sites in cubic Y_2O_3 host, C_2 (noncentrosymmetric) and C_{3i} (centrosymmetric),[9] as illustrated in Fig. 1. One of them consists of C_2 sites only, and the other contains equal numbers of C_2 and C_{3i} sites.[9]

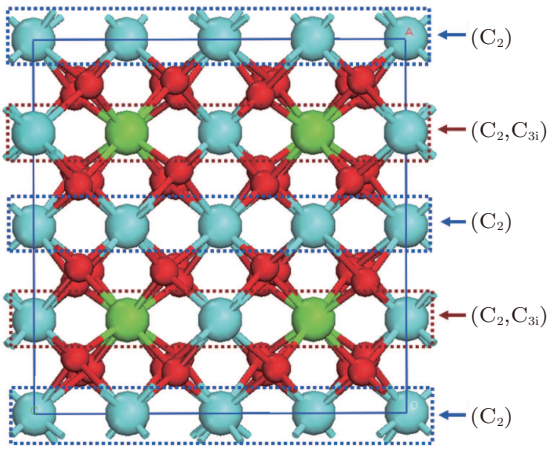


Fig. 1. (color online) Crystal structure of Y_2O_3 and arrangement of the two Y^{3+} symmetry sites (red color represents O atoms, green color represents Y atoms at C_{3i}, and light blue color represents Y atoms at C_2).

In general, the intra-configurational f–f electric dipole transitions are forbidden for centrosymmetric site because the levels have the same parity. In this case, only magnetic dipole transitions occur, which are much weaker than electric dipole transitions. For noncentrosymmetric sites, the crystal-field introduces an opposite-parity part to the potential energy of the crystal levels, which also makes the electric dipole transitions possible.[8,10] Therefore, for the Eu^{3+} located at C_{3i} (centrosymmetric) site, only the f–f magnetic dipole transitions can be observed. While for the case of Eu^{3+} ions at C_2 site, the electric dipole transitions are also allowed, which means that all the intraconfigurational f–f transitions can occur. The emission from Eu^{3+}(C_{3i}) site is not favorable because it only generates much lower (because of the lower probability of the transitions[11]) emission, and this also leads to the high probability of nonradiative relaxations, which would decrease the total emission efficiency. Thus, we would prefer emission from the Eu^{3+}at C_2 site for illumination purposes.

Nowadays, nanotechnology and nanoscience are emerging as leading topics in the technological revolution. The ability to engineer atoms on the nano-scale helps scientists to create tiny devices that can bring vast benefits to industry, such as reduced labor requirement and lower cost. To meet the requirement of tiny devices, the bulk phosphor material is no longer applicable. Thus, in the last decades, nano-sized phosphors have been investigated for their potential applications as well as their fundamental properties.[12–15] These nanomateri-

*Project supported by the National Natural Science Foundation of China (Grant Nos. 11304111 and 51172087), the Specialized Research Fund for the Doctoral Program of Higher Education of China (Grant No. 20110061110011), and the Postdoctoral Research Foundation of China (Grant No. 2013M541284).

†Corresponding author. E-mail: hongyangzhu@jlu.edu.cn

© 2014 Chinese Physical Society and IOP Publishing Ltd

als have a high surface to volume ratio, and the atoms at the surface have fewer neighbors than atoms in the bulk material, which lead to a different crystal field environment for the Eu^{3+} in the surface than that in the bulk material. In comparison with bulk material, the Y_2O_3:Eu^{3+} nanophosphor has different photoluminescence (PL) properties, such as the peak position, emission intensity, and lifetime. Therefore, it is essential to systematically study PL properties and energy transfer process of Y_2O_3:Eu^{3+} nanophosphors, although these properties of Y_2O_3:Eu^{3+} bulk material have been investigated.[16]

In this work, we systematically study optical properties of Y_2O_3:Eu^{3+} nanophosphors. The energy transfer process is presented by measuring the PL spectrum, PL excitation spectrum, and fluorescence decay curves. Specifically, we investigate the energy transfer processes between the Eu^{3+} in C_{3i} site and Eu^{3+}in C_2 site with the goal of improving the light emission efficiency and achieving better color quality.

2. Experimental details

Y_2O_3:Eu^{3+} nanophosphors with various Eu^{3+} concentrations (0.5 mol%, 1 mol%, 3 mol%, 5 mol%, 8 mol%, 12 mol%, and 15 mol%) were obtained by a glycine–nitrate solution combustion method. The process is designed as follows: the Y_2O_3 and Eu_2O_3 were dissolved in HNO_3 to obtain $Y(NO_3)_3$ and $Eu(NO_3)_3$ solutions, respectively. The obtained $Y(NO_3)_3$ and $Eu(NO_3)_3$ were mixed according to $(Y_{1-x}Eu_x)_2O_3$ and put into glycine ($C_2H_5NO_2$) solution. The mixture was stirred until a uniform solution was obtained. After this, the solution was heated to vaporize the water. When the water was almost dried out, the temperature roses quickly and the mixture was ignited at about 250 °C. The combustion was self-propagating until the glycine and nitrate were depleted. Y_2O_3:Eu^{3+} nanophosphors were formed after the combustion was completed.

The crystalline phase and the size of the Y_2O_3:Eu^{3+} nanophosphors were identified using a Rigaku D/max-2000 X-ray powder diffractometer with Cu Kα radiation (λ = 0.15405 nm). The emission and excitation spectra were measured using a Hitachi F-4500 fluorescence spectrometer with a 150-W xenon lamp as the excitation source. In the measurement of fluorescent dynamics and high resolution spectra (see Fig. 3(a)), a fourth-harmonic generator pumped by a pulsed Nd:YAG laser was used as an excitation source. The spectra was recorded by a Spex-1403 double raster monochromator with resolution of 0.005 nm, a photomultiplier, and a boxcar integrator, and processed by a computer. All of the measurements were performed at room temperature.

3. Results and discussion

3.1. XRD patterns and PL properties of Y_2O_3:Eu^{3+}

Figure 2 shows the XRD patterns of synthesized Y_2O_3:Eu^{3+} nanophosphors. All of the diffraction peaks are well indexed to cubic Y_2O_3 phase (JCPDS 43-1036), which was also plotted in Fig. 2 for comparison. No additional peaks belonging to other phases have been found. The particle size is 22 nm, which was calculated from the half-width of the peaks of the X-ray powder patterns by Scherrer's equation.

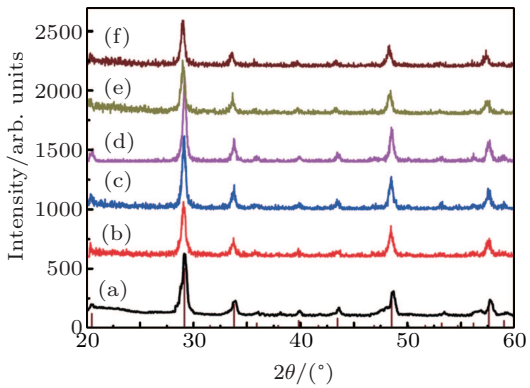


Fig. 2. (color online) The XRD patterns of $(Y_{1-x}Eu_x)_2O_3$. (a) x = 0.005, (b) x = 0.01, (c) x = 0.03, (d) x = 0.08, (e) x = 0.12, and (f) x = 0.15.

Figure 3(a) is a high-resolution spectrum of the 0.5% Eu^{3+}-doped Y_2O_3 nanophosphor under the fourth harmonic (266 nm) of Nd:YAG laser excitation. All the peaks belong to the $^5D_0 \rightarrow {}^7F_j$ (j = 0, 1, 2, 3, 4) transition of Eu^{3+}. Among them, the emission at 580 nm is assigned to the $^5D_0 \rightarrow {}^7F_0$ transition of Eu^{3+}. The emissions at 582 nm and 592 nm are assigned to the $^5D_0 \rightarrow {}^7F_1$ transition of Eu^{3+} at C_{3i} site. The emissions at 587 nm, 593 nm, and 600 nm are assigned to the $^5D_0 \rightarrow {}^7F_1$ transition of Eu^{3+} at C_2 site (see Fig. 3(c)). The strongest emission centered at 611 nm originates from the $^5D_0 \rightarrow {}^7F_2$ transition of the Eu^{3+} at C_2 site. The corresponding PL excitation spectrum by monitoring the 611 nm emission shows two broad bands and several sharp peaks (see Fig. 3(b)). The band centered at 211 nm is excitonic absorption due to the $O^{2-} \rightarrow Y^{3+}$ electron transfer transition. The excitation band centered at 250 nm is attributed to the $O^{2-} \rightarrow Eu^{3+}$ charge transfer (CT) transition.[17] The weaker absorption peaks between 300 nm and 500 nm belong to the $f \rightarrow f$ transition of Eu^{3+}.

3.2. Emission spectra of Y_2O_3:Eu^{3+}phosphors under excitation of 239 nm with various Eu^{3+}concentrations

In order to investigate the optical properties of Y_2O_3:Eu^{3+} nanophosphors, the emission spectra of Y_2O_3:Eu^{3+} nanophosphors with various Eu^{3+} concentrations

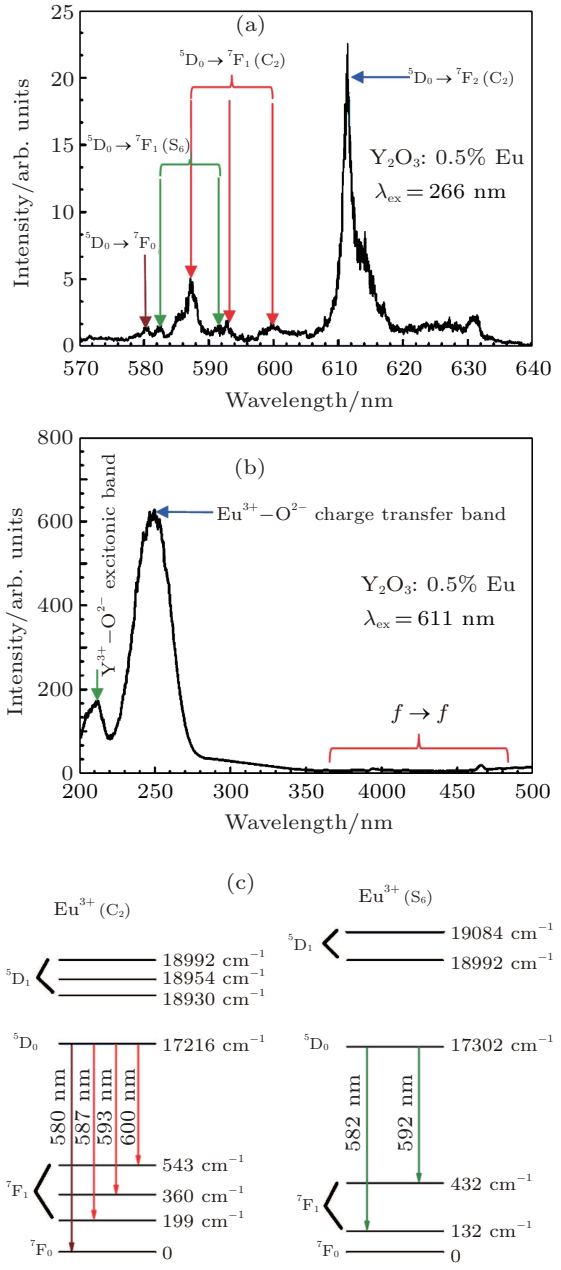


Fig. 3. (color online) (a) High-resolution PL emission spectrum of 0.5% Eu^{3+}-doped Y_2O_3 under 266 nm excitation. (b) The corresponding excitation spectrum monitoring 611 nm emission. (c) A schematic of energy levels of Eu^{3+} (C_2) and Eu^{3+} (C_{3i}) for the lowest manifold of the ^5D and ^7F terms in Y_2O_3:Eu^{3+}.

were measured. Figure 4(a) shows the emission spectra (530–540 nm) of the Y_2O_3:Eu^{3+} with various Eu^{3+} concentrations under 239-nm excitation, which were normalized by 611-nm emission for comparison. Note that all of the spectra were offset by a certain number. The emissions between 530–540 nm are assigned to radiative emission from the $^5D_1$ of Eu^{3+} at C_{3i} site. All of the spectra are very similar and contain almost similar features. However, the intensity ratio of these emissions to the strongest hypersensitive $^5D_0 \rightarrow {}^7F_2$ line at 611 nm, this is the emission of Eu^{3+} occupying C_2 site, which systematically decreases with the increase in Eu^{3+} concentration. This indicates that the ratio of C_{3i} site emission to that of the C_2 site decreases with the increase in the Eu^{3+} concentration. In the region of 575–582 nm (see Fig. 4(b)), it can be well fitted with two Gaussian profiles: one is peaking at 580 nm, which is from Eu^{3+} at C_2 emission, and the other is centering at 582 nm from Eu^{3+} at C_{3i} emission. It can be seen that the relative emission intensity ratio of C_{3i} site to C_2 site decreases with increasing Eu^{3+} concentration. That is, when the Eu^{3+} concentration increases, the $Eu^{3+}(C_2)$ luminescence intensity increases with the expense of the $Eu^{3+}(C_{3i})$ emission. This is attributed to the energy transfer from the C_{3i} site to the C_2 site, as happened in the bulk materials. The distance between Eu^{3+} decreases with the increase in the Eu^{3+} concentration which enhances the probability of energy transfer of $Eu^{3+}(C_{3i}) \rightarrow Eu^{3+}(C_2)$. Therefore, the ratio of the emission intensity of the C_{3i} site to the C_2 site decreases with increasing Eu^{3+} concentration.

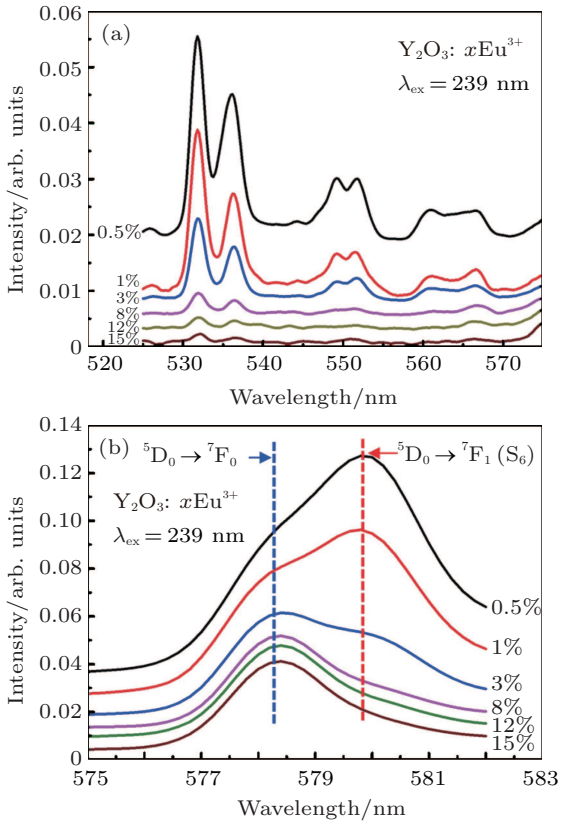


Fig. 4. (color online) Emission spectra (normalized by 611 nm emission) of the Y_2O_3:Eu^{3+} with various Eu^{3+} concentrations (a) in the range of 525–575 nm, and (b) in the range of 575–582 nm.

3.3. Excitation spectra of Y_2O_3:Eu^{3+} with various Eu^{3+} concentrations

In addition to the emission spectra, the excitation spectra were also measured to investigate the optical properties of Y_2O_3:Eu^{3+} nanophosphors. As shown in Fig. 3(c), Eu^{3+} occupying C_{3i} site has higher energy levels than that of Eu^{3+} at C_2 sites, as illustrated. Therefore, the corresponding excitation spectra should be different. Based on this consideration,

the PL excitation spectra were also measured for Y_2O_3:Eu^{3+} with various Eu^{3+} concentrations by monitoring 582-nm and 611-nm emissions.

Figure 5 shows the normalized excitation spectra by monitoring the 611-nm and 582-nm emissions of Y_2O_3:Eu^{3+} with various Eu^{3+} concentrations. In the case of Y_2O_3:Eu^{3+} with lower Eu^{3+} concentrations, the possible Eu^{3+}–Eu^{3+} interaction can be negligible due to the long distance between Eu^{3+}. The excitation spectra by monitoring 611-nm and 582-nm emissions are different in CT regions (see Figs. 5(a) and 5(b)).

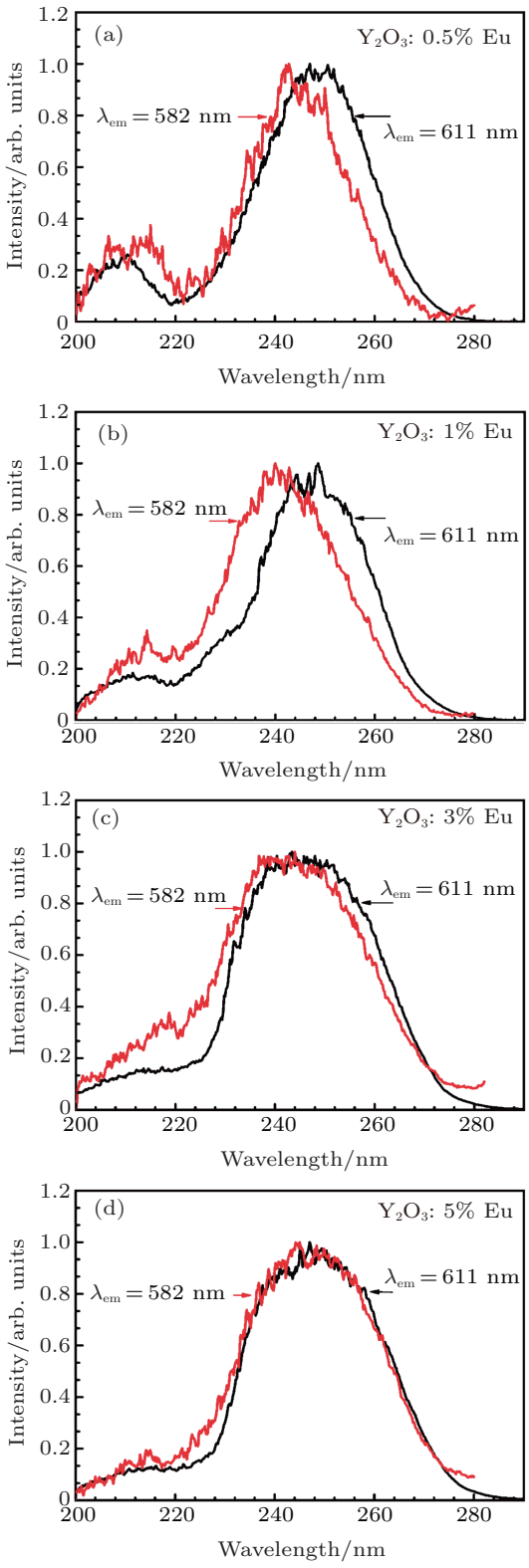


Fig. 5. (color online) Excitation spectra of Y_2O_3:Eu^{3+} with various Eu^{3+} concentrations (the red line monitors the 580-nm emission and the black line monitors the 609-nm emission).

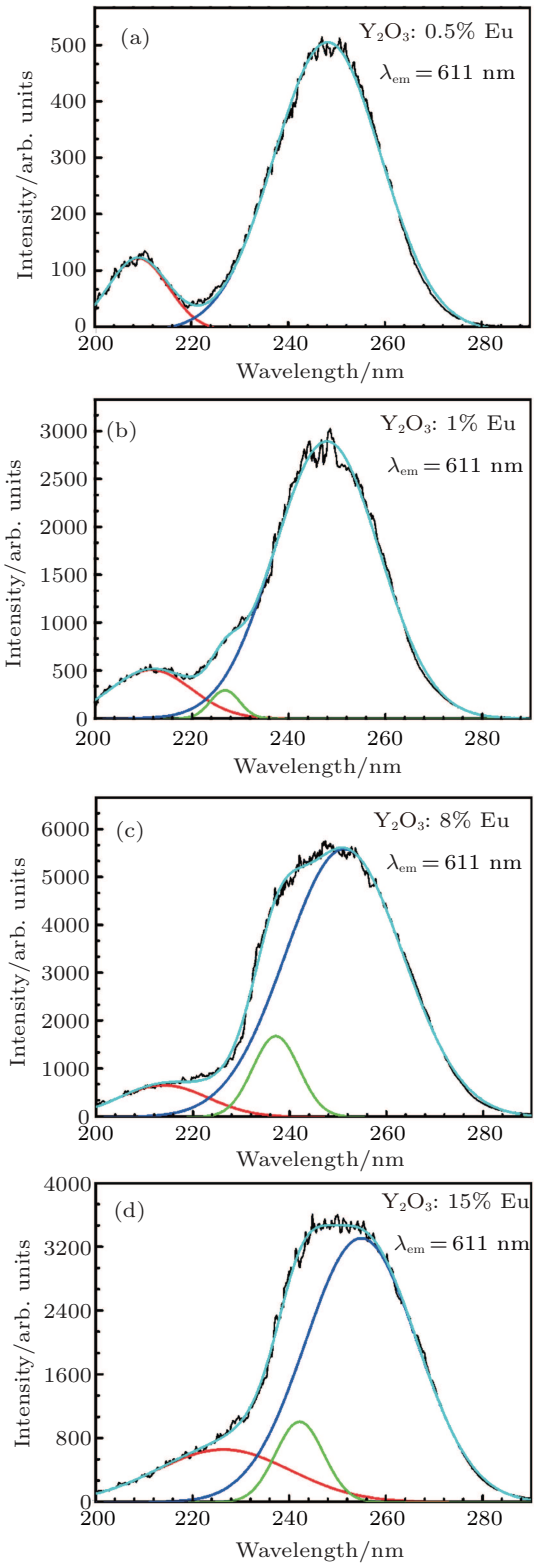


Fig. 6. (color online) Fitted excitation spectra monitoring the 611-nm emission with various Eu^{3+} concentrations: (a) 0.5%, (b) 1%, (c) 8%, (d) 15%.

For the 582-nm emission ($Eu^{3+}(C_{3i})$), the CT band located in higher energy region shows a peak around 239 nm. Meanwhile, for the 611-nm emission the peak was shifted toward lower energies, peaking around 251 nm. These two bands get closer and closer with the increase in the Eu^{3+} concentration. This is attributed to the energy transfer between the $Eu^{3+}(C_{3i})$ and $Eu^{3+}(C_2)$. In order to trace the change of excitation spectra with the increase in the Eu^{3+} concentration, the CT bands by monitoring 611-nm emission were fitted using Gaussian curve, as shown in Fig. 6. At a lower concentration (0.5% mol Eu^{3+}), the excitation spectrum can be fitted well with two excitation bands: one is the excitation absorption centered at 210 nm;[18] the other is the CT band of Eu^{3+} (C_2) peaking at 251 nm. When the Eu^{3+} concentration increased to 1 mol%, it must be fitted with three Gaussian curves. In addition to the excitation absorption centered at 210 nm and the CT band from the Eu^{3+} (C_2), the CT band from Eu^{3+} (C_{3i}) centered at 239 nm is also observed. The ratio of the intensity of absorption from $Eu^{3+}(C_{3i})$ to that from $Eu^{3+}(C_2)$ increases with increasing Eu^{3+} concentrations. This indicates the increasing rate of the energy transfer from the excited $Eu^{3+}(C_{3i})$ to the nearby located $Eu^{3+}(C_2)$ ions.

3.4. Fluorescence dynamics of Y_2O_3:Eu^{3+} nanophosphors with various Eu^{3+} concentrations

The fluorescence decay curves were also measured to further understand the optical properties of Y_2O_3:Eu^{3+} nanophosphors. Florescence decay curves of $^5D_0$ energy level were measured for both 582-nm emission and 611-nm emission, corresponding to $^5D_0 \rightarrow ^7F_1$ of Eu^{3+} at C_{3i} site and $^5D_0 \rightarrow ^7F_2$ of Eu^{3+} at C_2 site, respectively. Figure 7(a) is the normalized fluorescence decay curves of the emissions of $^5D_0$ which is measured by monitoring the 582 nm emission, which belongs to the $^5D_0 \rightarrow ^7F_1$ transition of $Eu^{3+}(C_{3i})$, in the Y_2O_3:Eu^{3+} with various Eu^{3+} concentrations. As we can see, the lifetime of Eu^{3+} occupying the C_{3i} site is 5.51 ms, 4.65 ms, 3.08 ms, 1.43 ms, and 1.18 for the Eu^{3+} concentrations of 0.5%, 1%, 3%, 8%, and 12%, respectively. The fluorescence lifetime decreases with the increase in Eu^{3+} concentration and dramatically drops when the Eu^{3+} concentration increases to 8 mol% (see Fig. 7(c)). The lifetimes of Eu^{3+} in the C_2 site are 1.94 ms, 1.93 ms, 1.90 ms, 1.72 ms, and 1.38 ms for the Eu^{3+} concentration of 0.5%, 1%, 3%, 8%, and 12%, respectively. Compared to the lifetime of Eu^{3+}at C_{3i} site, there are only small changes for the lifetime of 611 nm emission. Only when the Eu^{3+} concentration increases to 8 mol% is a relatively dramatical drop observed. This is attributed to the increased energy transfer between $Eu^{3+}(C_2)$ and $Eu^{3+}(C_2)$ in Y_2O_3 nanoparticles (see Figs. 7(b) and 7(c)). To understand the underlying mechanism, we should also recall that the Eu^{3+}at two symmetry sites have different lifetimes. When the concentration of Eu^{3+} is 0.5% mole, the distance between the Eu^{3+} is very large. Therefore, there is almost no interaction between the Eu^{3+} ions, thus the lifetime of Eu^{3+} at the C_{3i} site is long. However, the distances between the Eu^{3+} ions becomes shorter and shorter with the increase in Eu^{3+} concentrations and the interaction between the Eu^{3+} ions became stronger and stronger. This increases the energy transfer chance between $Eu^{3+}(C_{3i})$ and $Eu^{3+}(C_2)$. This also confirms that the energy of excited ions of Eu^{3+} located at the C_{3i} site can be transferred into the $Eu^{3+}(C_2)$ ions that are located nearby. This process becomes more and more efficient as the Eu^{3+} concentration increases.

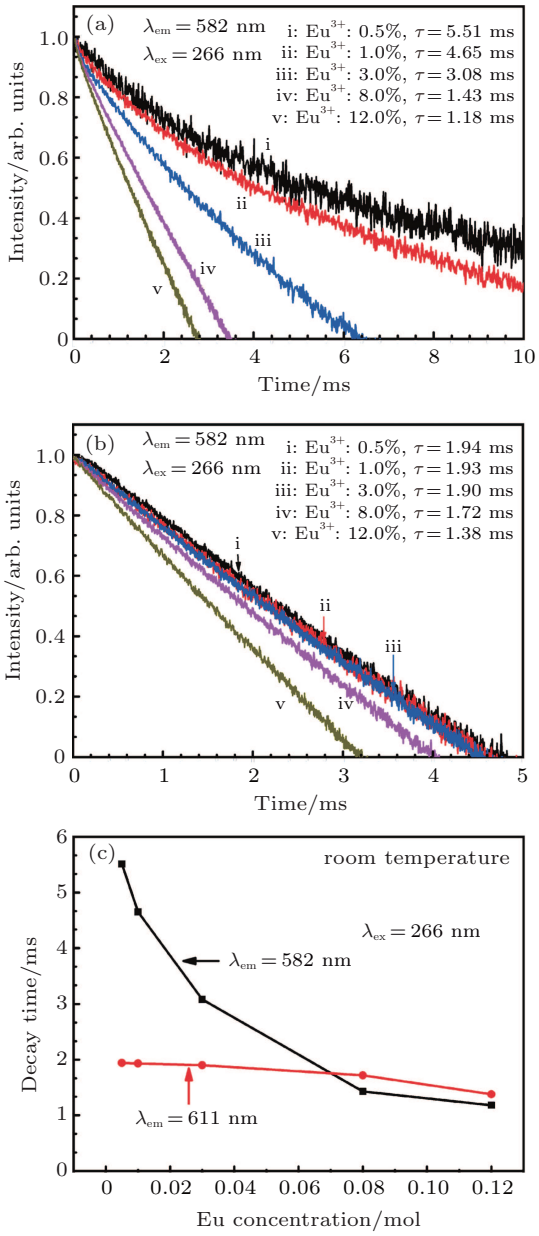


Fig. 7. (color online) (a) Normalized fluorescence decay curves of the $^5D_0$ emission by monitoring 582-nm emission in the Y_2O_3:Eu^{3+} phosphors with various Eu^{3+} concentrations under 266-nm excitation. (b) Normalized fluorescence decay curves of the $^5D_0$ emission by monitoring 611-nm emission in the Y_2O_3:Eu^{3+} phosphors with various Eu^{3+} concentrations under 266-nm excitation. (c) Concentration dependence of fluorescence lifetime derived from the analytical fits to the decay curves of 582-nm and 611-nm emissions.

Another point to be emphasized is that when the Eu^{3+} concentration is lower, the lifetime of 582-nm emission is longer than that of 611-nm emission. However, the fluorescence lifetime of 582-nm emission is shorter than that of 611-nm emission when the Eu^{3+} concentration increases to 8 mol% (see Fig. 7(c)). This also relates to the energy transfer between Eu^{3+} in two symmetry sites. As previously mentioned, the 582-nm and 612-nm emissions are attributed to emissions from $Eu^{3+}(C_{3i})$ and $Eu^{3+}(C_2)$ sites, respectively.

4. Conclusion

Cubic Y_2O_3:Eu^{3+} nanophosphors with various Eu^{3+} concentrations were synthesized by a simple combustion method. The spectroscopic measurements were employed to trace the energy transfer between Eu^{3+} ions at C_{3i} site and C_2 site. The energy transfer was confirmed by measuring the emission spectrum, excitation spectrum, and fluorescence decay curves. The ratio of 582-nm ($Eu^{3+}(C_{3i})$) emission to $^5D_0 \rightarrow ^7F_2$ emission systematically decreases with the increase in the Eu^{3+} concentration. The changes of emission spectra are attributed to the energy transfer from the $Eu^{3+}(C_{3i})$ to $Eu^{3+}(C_2)$. The excitation spectra of lower Eu^{3+}-doped samples demonstrate that the energy level of Eu^{3+} (C_{3i}) is higher than that of the $Eu^{3+}(C_2)$. The changes of excitation spectra with the Eu^{3+} concentration also indicate that there is an energy transfer from the $Eu^{3+}(C_{3i})$ to the $Eu^{3+}(C_2)$. The energy transfer of Eu^{3+} from C_{3i} site to C_2 site is especially important because the Eu^{3+} at C_2 has much higher radiative efficiency and better color quality for a variety of applications, such as illumination and display technology.

References

[1] Zhu H, Ma Y, Yang H, Zhu P, Du J, Ji C and Hou D 2010 *Solid State Commun.* **150** 1208
[2] Zhang J, Cui H, Zhu P, Ma C, Wu X, Zhu H, Ma Y and Cui Q 2014 *J. Appl. Phys.* **115** 023502
[3] Lü Q, Zhao L, Guo F and Li M 2009 *Chin. Phys. B* **18** 4030
[4] Ray S, Pramanik P, Singha A and Roy A 2005 *J. Appl. Phys.* **97** 94312
[5] Konrad A, Fries T, Gahn A, Kummer F, Herr U, Tidecks R and Samwer K 1999 *J. Appl. Phys.* **86** 3129
[6] Qi Z M, Shi C S, Zhang W W, Zhang W P and Hu T D 2002 *Appl. Phys. Lett.* **81** 2857
[7] Rakov N, Lozano W, Maciel G S and De Araujo C B 2006 *Chem. Phys. Lett.* **428** 134
[8] Judd B R 1962 *Phys. Rev.* **127** 750
[9] Chang N C and Gruber J B 1964 *J. Chem. Phys.* **41** 3227
[10] Buijs M, Meyerink A and Blasse G 1987 *J. Lumin.* **37** 9
[11] Zych E, Karbowiak M, Domagala K and Hubert S 2002 *J. Alloy. Compd.* **341** 381
[12] Reddy A A, Das S, Goel A, Sen R, Siegel R, Mafra L, Prakash G V and Ferreira J M F 2013 *AIP Adv.* **3** 022126
[13] Dai Q L, Foley M E, Breshike C J, Lita A and Strouse G F 2011 *J. Am. Chem. Soc.* **133** 15475
[14] Shang C Y, Wang X Q, Kang H and Han D M 2011 *J. Appl. Phys.* **109** 104309
[15] Krishna R H, Nagabhushana B M, Nagabhushana H, Murthy N S, Sharma S C, Shivakumara C and Chakradhar R P S 2013 *J. Phys. Chem. C* **117** 1915
[16] Forest H and Ban G 1969 *J. Electrochem. Soc.* **116** 474
[17] Dhanaraj J, Jagannathan R, Kutty T R N and Lu C H 2001 *J. Phys. Chem. B* **105** 11098
[18] Jollet F, Noguera C, Thromat N, Gautier M and Duraud J P 1990 *Phys. Rev. B* **42** 7587